International Journal of
Molecular Sciences

MDPI

Article

Antiviral Activity of N_1,N_3-Disubstituted Uracil Derivatives against SARS-CoV-2 Variants of Concern

Andrei E. Siniavin [1,2,*,†], Mikhail S. Novikov [3,†], Vladimir A. Gushchin [1,4,*], Alexander A. Terechov [1], Igor A. Ivanov [1,2], Maria P. Paramonova [3], Elena S. Gureeva [3], Leonid I. Russu [1], Nadezhda A. Kuznetsova [1], Elena V. Shidlovskaya [1], Sergei I. Luyksaar [1], Daria V. Vasina [1], Sergei A. Zolotov [1], Nailya A. Zigangirova [1], Denis Y. Logunov [1] and Alexander L. Gintsburg [1,5]

1 N.F. Gamaleya National Research Center for Epidemiology and Microbiology, Ivanovsky Institute of Virology, Ministry of Health of the Russian Federation, 123098 Moscow, Russia
2 Department of Molecular Neuroimmune Signalling, Shemyakin-Ovchinnikov Institute of Bioorganic Chemistry, Russian Academy of Sciences, 117997 Moscow, Russia
3 Department of Pharmaceutical & Toxicological Chemistry, Volgograd State Medical University, 400131 Volgograd, Russia
4 Department of Virology, Lomonosov Moscow State University, 119991 Moscow, Russia
5 Department of Infectiology and Virology, Federal State Autonomous Educational Institution of Higher Education I M Sechenov First Moscow State Medical University of the Ministry of Health of the Russian Federation (Sechenov University), 119435 Moscow, Russia
* Correspondence: andreysi93@ya.ru (A.E.S.); wowaniada@yandex.ru (V.A.G.)
† These authors contributed equally to this work.

check for updates

Citation: Siniavin, A.E.; Novikov, M.S.; Gushchin, V.A.; Terechov, A.A.; Ivanov, I.A.; Paramonova, M.P.; Gureeva, E.S.; Russu, L.I.; Kuznetsova, N.A.; Shidlovskaya, E.V.; et al. Antiviral Activity of N_1,N_3-Disubstituted Uracil Derivatives against SARS-CoV-2 Variants of Concern. *Int. J. Mol. Sci.* **2022**, *23*, 10171. https://doi.org/10.3390/ijms231710171

Academic Editor: Kohji Noguchi

Received: 9 August 2022
Accepted: 25 August 2022
Published: 5 September 2022

Publisher's Note: MDPI stays neutral with regard to jurisdictional claims in published maps and institutional affiliations.

Abstract: Despite the widespread use of the COVID-19 vaccines, the search for effective antiviral drugs for the treatment of patients infected with SARS-CoV-2 is still relevant. Genetic variability leads to the continued circulation of new variants of concern (VOC). There is a significant decrease in the effectiveness of antibody-based therapy, which raises concerns about the development of new antiviral drugs with a high spectrum of activity against VOCs. We synthesized new analogs of uracil derivatives where uracil was substituted at the N_1 and N_3 positions. Antiviral activity was studied in Vero E6 cells against VOC, including currently widely circulating SARS-CoV-2 Omicron. All synthesized compounds of the panel showed a wide antiviral effect. In addition, we determined that these compounds inhibit the activity of recombinant SARS-CoV-2 RdRp. Our study suggests that these non-nucleoside uracil-based analogs may be of future use as a treatment for patients infected with circulating SARS-CoV-2 variants.

Keywords: SARS-CoV-2; COVID-19; antiviral agents; non-nucleoside inhibitor; RNA-dependent RNA polymerase

1. Introduction

The ongoing coronavirus disease 2019 (COVID-19) pandemic caused by severe acute respiratory syndrome coronavirus 2 (SARS-CoV-2) is a global public health crisis [1]. SARS-CoV-2 is a positive-sense, single-stranded RNA virus [2]. Like other coronaviruses [3], SARS-CoV-2 synthesizes a variety of viral enzymes and proteins that are essential for viral entry, replication, and pathogenesis, including structural and non-structural proteins [4]. As the pandemic progresses, several new variants of the virus emerged [5]. Five «variants of concern» (VOCs) (alpha, beta, gamma, delta, and omicron) have been described that are associated with increased virus transmission, virulence, or immune evasion (https://www.ecdc.europa.eu/en/COVID-19/variants-concern accessed on 28 April 2022). The development of effective antiviral drugs is a promising strategy [6]. Recently conducted randomized clinical trials identified antiviral drugs that target SARS-CoV-2. Remdesivir, molnupiravir, and nirmatrelvir have recently exhibited clinical benefits when administered early on during COVID-19 infection [7–9]. However, the number of substances with a

proven antiviral effect against coronaviruses is still insufficient. Thus, as new variants of the virus with various mutations in the genome of the virus appear, resistance to antiviral drugs may develop. It is necessary to develop adequate combination therapy schemes and a reserve of active substances to counteract the loss of effectiveness in a timely manner.

One of the main molecular targets of viruses is their polymerase and replicative complex. Combinations of nucleoside and non-nucleoside reverse transcriptase inhibitors have been successfully used to treat HIV infection [10]. The main approach to the development of new antiviral drugs against SARS-CoV-2, like other viruses, is based on targeting RNA-dependent RNA polymerase (RdRp) [11,12]. For example, remdesivir is a potent nucleoside polymerase inhibitor of SARS-CoV-2 and MERS-CoV [13,14]. However, the mechanism of action of nucleoside inhibitors is based on chain termination and the mutation of viral progeny, which can lead to drug resistance and host genetic toxicity [15,16]. Therefore, the activity of new non-nucleoside antiviral drugs targeting viral polymerase against various viral infections is widely studied.

Previously, the antiviral activity of various non-nucleoside uracil derivatives was demonstrated. These compounds inhibited the replication of HCMV [17], VZV [18], HIV [19] and HCV [20]. Moreover, ramified derivatives of uracil presented antiviral activity against tick-borne encephalitis virus (TBEV) [21]. In the present study, we evaluated the antiviral activity of novel uracil derivatives against SARS-CoV-2 in vitro to determine their potential for further study as novel antiviral compounds against SARS-CoV-2 infection.

2. Results

2.1. Chemical Synthesis of Panel Compounds

The target acids were synthesized by treating the starting 1-(naphthalen-1-ylmethyl)uracil (**1**) [22], 1-(naphthalen-2-ylmethyl)uracil (**2**) [22], 1-(4-bromonaphthalen-1-ylmethyl)uracil (**3**) [22], 1-(anthrecen-9-ylmethyl)uracil (**4**) [23], 1-[3-(4-bromophenoxy)propyl]uracil (**5**) [24], 1-[5-(4-fluorophenoxy)pentyl]uracil (**6**), 1-[5-(2-bromophenoxy)pentyl]uracil (**7**) [25], 1-[5-(4-bromo-phenoxy)pentyl]uracil (**8**) [24], 1-[5-(3,5-dimethylphenoxy)pentyl]uracil (**9**) [26] or 1-[12-(4-bromophenoxy)dodecyl]uracil (**10**) [17] with an equimolar amount of 4-(ω-bromoalkoxy)benzoic acid methyl ester (**11–13**) in DMF solution in the presence of K_2CO_3. The resulting 1,3-disubstituted uracil without further purification was subjected to alkaline hydrolysis in an aqueous-alcoholic solution, which led to the formation of the corresponding benzoic acids (Scheme 1).

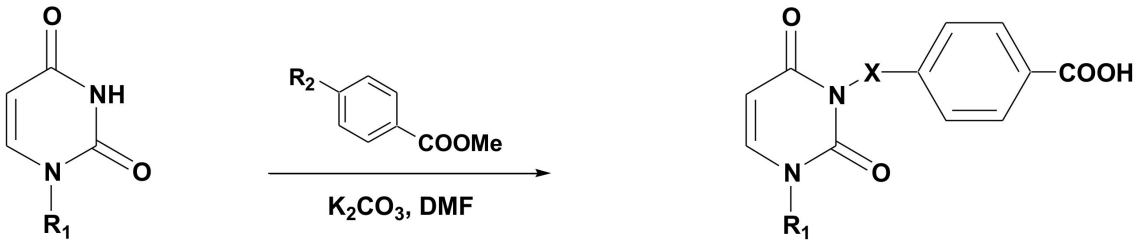

1 R_1 = naphthyl-1-methyl
2 R_1 = naphthyl-2-methyl
3 R_1 = 4-bromonaphthyl-1-methyl
4 R_1 = anthracenyl-9-methyl
5 R_1 = 3-(4-bromophenoxy)propyl
6 R_1 = 5-(4-fluorophenoxy)pentyl
7 R_1 = 5-(2-bromophenoxy)pentyl
8 R_1 = 5-(4-bromophenoxy)pentyl
9 R_1 = 5-(3,5-dimethylphenoxy)pentyl
10 R_1 = 12-(4-bromophenoxy)dodecyl

11 R_2 = $O(CH_2)_3Br$
12 R_2 = $O(CH_2)_4Br$
13 R_2 = $O(CH_2)_5Br$

Z601 R_1 = naphthyl-1-methyl, X = $(CH_2)_4O$;
Z870 R_1 = 5-(4-fluorophenoxy)pentyl, X = $(CH_2)_5O$;
Z871 R_1 = 5-(2-bromophenoxy)pentyl, X = $(CH_2)_5O$;
Z873 R_1 = 3-(4-bromophenoxy)propyl, X = $(CH_2)_4O$;
Z874 R_1 = 5-(3,5-dimethylphenoxy)pentyl, X = $(CH_2)_5O$;
Z876 R_1 = anthracenyl-9-methyl, X = $(CH_2)_5O$;
Z1005 R_1 = naphthyl-2-methyl, X = $(CH_2)_4O$;
Z1006 R_1 = 4-bromonaphthyl-1-methyl, X = $(CH_2)_4O$;
Z1007 R_1 = 12-(4-bromophenoxy)dodecyl, X = $(CH_2)_3O$

Scheme 1. Synthesis of Compounds.

In addition, we obtained a thymine derivative, the synthesis of which consisted of the treatment starting with 1-[5-(4-bromophenoxy)pentyl]thymine (**14**) [24] and an equimolar amount of 4-(5-bromopentyloxy)benzoic acid methyl ester (**13**) in DMF solution in the presence of K_2CO_3. The resulting 1,3-disubstituted thymine without further purification was subjected to alkaline hydrolysis in an aqueous-alcoholic solution, which produced the target benzoic acid **872** (Scheme 2).

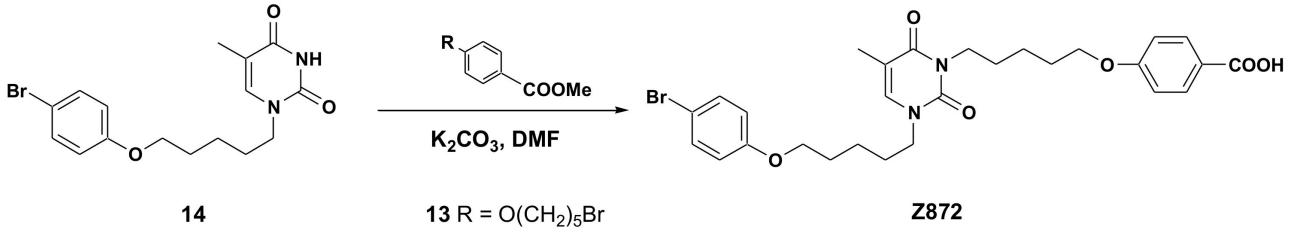

Scheme 2. Synthesis of Compound **872**.

Next, we synthesized a uracil derivative linked to a benzoic acid residue by a methylene group. The synthesis of this compound was carried out by treatment starting with 1-[5-(4-bromo-phenoxy)pentyl]uracil (**8**) and an equimolar amount of 4-chloromethylbenzoic acid methyl ester (**15**) followed by alkaline hydrolysis in an aqueous-alcoholic medium. As a result, the target benzoic acid 875 was obtained at a 77% yield. (Scheme 3).

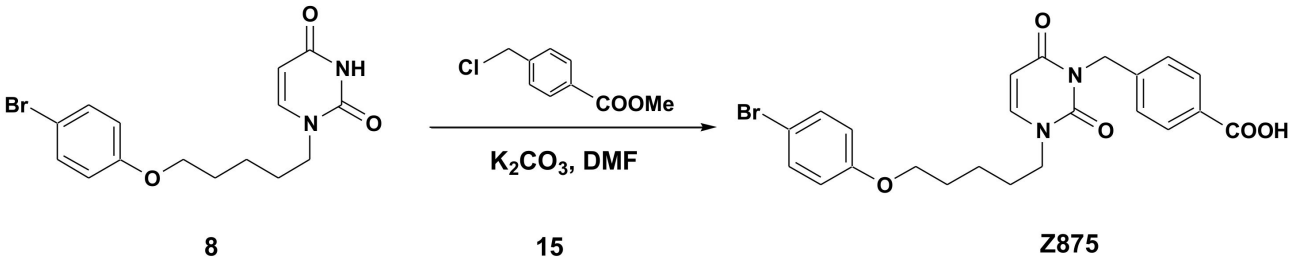

Scheme 3. Synthesis of Compound **875**.

We also obtained an analog of compound **876**, which did not contain a carboxyl group in the side chain. Its synthesis was carried out by the treatment of 1-(anthrecen-9-ylmethyl)uracil (**4**) with an equimolar amount of 1-bromo-4-[(6-bromohexyl)oxy]benzene (**16**) in DMF solution in the presence of K_2CO_3. In this case, the target compound **611** was formed, the yield of which was 66% (Scheme 4).

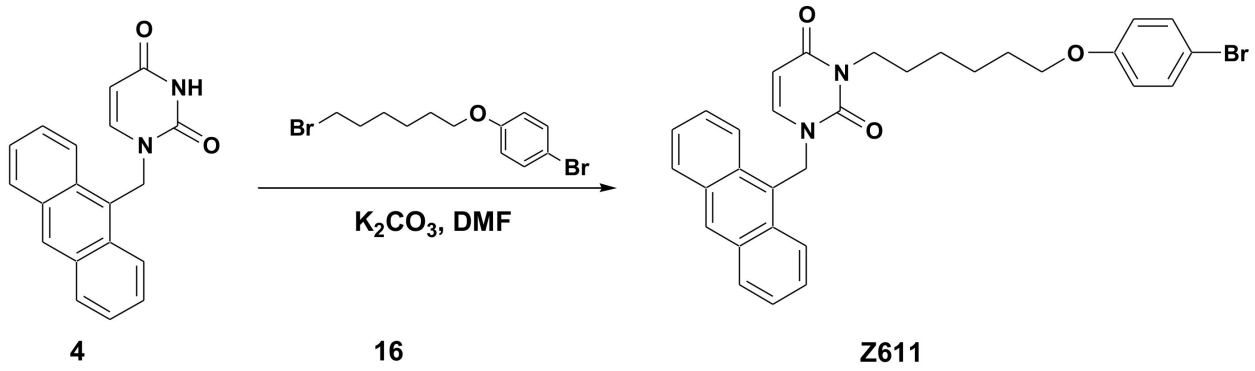

Scheme 4. Synthesis of Compound **611**.

2.2. Antiviral Activity

To study the antiviral effect of the compounds (Figure 1), Vero E6 cells were treated with the indicated concentrations and infected with the Delta (B.1.617.2) or Beta (B.1.351)

variants of SARS-CoV-2. Antiviral activity was based on an analysis of the virus-induced cytopathic effect (CPE). The data obtained showed that the IC_{50} values ranged from 13.3 to 49.97 μM (Figure 1, Table 1). To determine the cytotoxicity of compounds, Vero E6 cells treated with test compounds were subjected to an MTT assay. The results demonstrate that most compounds do not significantly reduce cell viability and CC_{50} values were >50 μM. However, several compounds (**871**, **874** and **1007**) reduced cell proliferation without significant cell death.

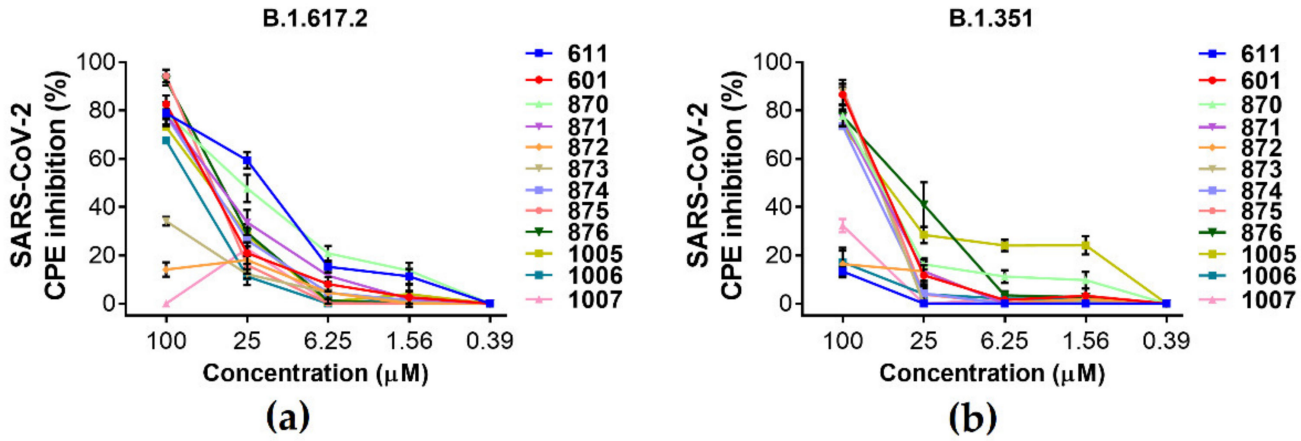

Figure 1. Antiviral Activity of Compounds against (**a**) «Delta» and (**b**) «Beta» Variants of the SARS-CoV-2. Vero E6 Cells were Treated with Various Compound Concentrations and Infected with SARS-CoV-2 at 100 $TCID_{50}$. The virus-induced cytopathic effect (CPE) was measured at 72 h post-infection using the MTT test. Points and error bars represent mean ± SEM of triplicate measurements.

Table 1. Values of CC50 and IC50 against SARS-CoV-2 (Delta, Beta and Omicron) Infection of Vero E6 cells.

N	IC_{50} (μM)			CC_{50} (μM)
	B.1.617.2	B.1.351	B.1.1.529	
601	32.72	32.68	27.1	>50
611	13.3	>50	>50	>50
870	14.6	34.14	24.42	>50
871	26.57	27.33	>50	>25
872	>50	>50	7.92	>50
873	>50	49.97	28.21	>50
874	30.24	29.06	>50	>25
875	30.66	33.06	22.55	>50
876	29.33	23.82	22.39	>50
1005	27.83	15.45	>50	>50
1006	27.44	>50	>50	>50
1007	>50	>50	>50	>25

We also confirmed the inhibitory effect of the compounds on the infection of the SARS-CoV-2 Omicron BA.1.1 using a plaque reduction assay (Figure 2). To assess their antiviral activity, half-maximal inhibitory doses (IC_{50}) were determined. It is interesting to note that of the twelve compounds tested, only six showed a pronounced antiviral effect. The calculated IC_{50} values for these compounds ranged from 7.92 μM to 28.21 μM (Table 1).

To explore which steps of the SARS-CoV-2 replication cycle were interrupted by the test compounds, we performed a time-of-drug-addition assay for compounds **874** and **876**, which were selected as representatives with different substituents at positions N_1 and N_3. Cells were treated with 25 μm of these compounds at various stages of infection (entry, full time and post-entry) which was followed by qRT-PCR assays. The addition of compounds at the «entry» step did not inhibit the production of viral RNA (Figure 3).

However, the addition of compounds at the «full time» step inhibited virus replication, resulting in a decrease in the viral load in the supernatant of infected Vero E6 cells. In addition, compound **876** reduced the viral load at the «post-entry» stage.

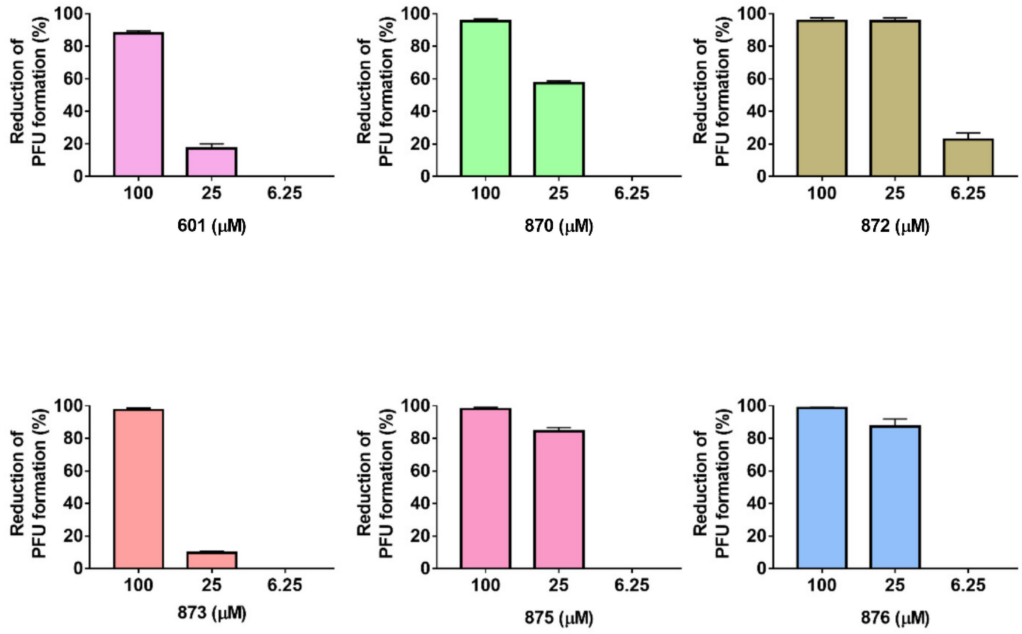

Figure 2. Antiviral Efficacy of Test Compounds in a Plaque Reduction Assay against Omicron SARS-CoV-2. Various dilutions of the test compounds were added to Vero E6 cells, after which the cells were infected with 50 p.f.u./well for 1 h. Then, the residual virus was removed and the cells were overlaid with 0.7% CMC containing the indicated dilutions of the compounds. After 72 h of infection, the wells were fixed with formalin, stained with crystal violet, and plaques were counted. Results are representative of $n = 3$ and are mean ± SEM.

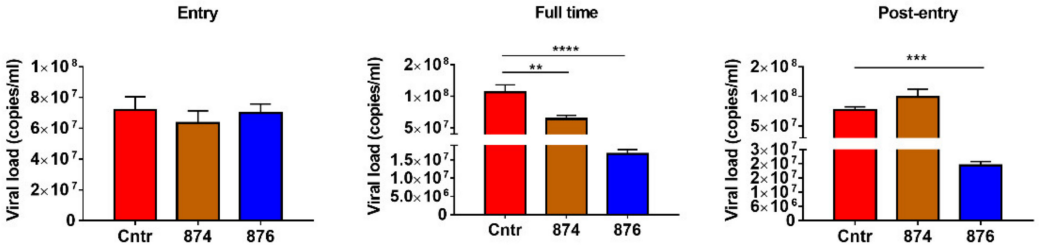

Figure 3. Time-of-drug-addition Assay. Vero E6 cells were treated with the compounds at different time points of the viral replication cycle as described in the Materials and Methods chapter. For all experimental groups, cells were infected with SARS-CoV-2 at an MOI of 0.01. Viral RNA copies in the supernatant were quantified by qRT-PCR at 18 h post-infection. All results are shown as mean ± SEM ($n = 3$). One-way ANOVA with Tukey's post hoc test: ** $p < 0.01$, *** $p < 0.001$ and **** $p < 0.0001$.

2.3. Mechanism of Action and Inhibition of SARS-CoV-2 RdRp

Molecular docking and the mean values of docking scores, as well as binding to SARS-CoV-2 RdRp were evaluated for all tested compounds. Due to the hydrophobic nature of uracil derivatives, the sites of interest are expected to be mostly hydrophobic too. One of such sites that may directly affect enzyme functions is the RNA cleft that features some non-polar cavities. This cleft is already being used as one of the docking targets by te hD3Pharma "D3Targets 2019-nCov" web server project [27]. The best score of 8.3 corresponds to **876** (Figure 4), so we docked it with an RNA cleft (Figure 5). Its closest

anthracyl (**611**) and naphthyl (**1006** and **601**) analogs were predicted to have scores from -7.5 to -6.9, and the other compounds' binding was worse.

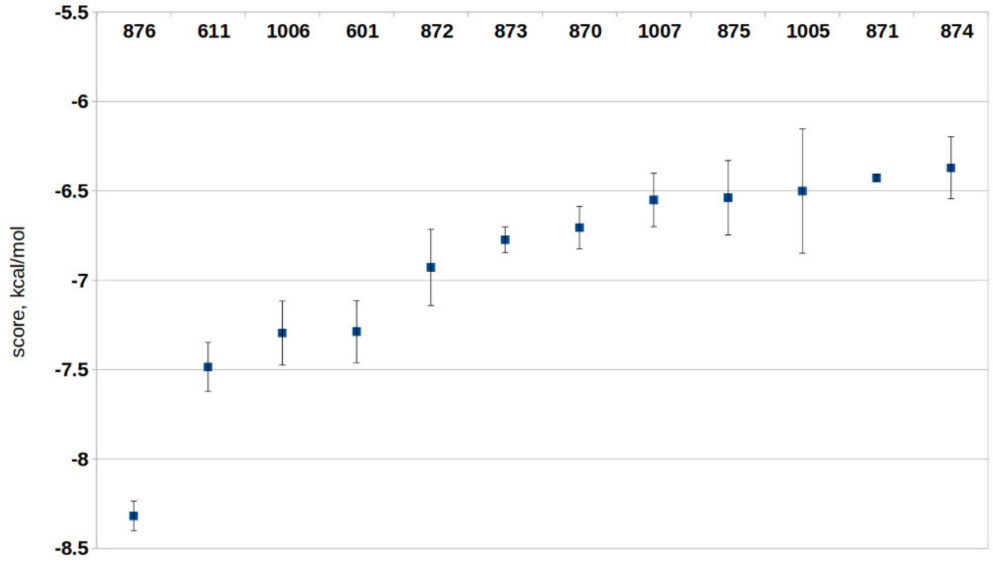

Figure 4. Molecular Docking Results, Average Values from 4 Runs. Compounds are sorted from lowest to highest score values (lowers are better).

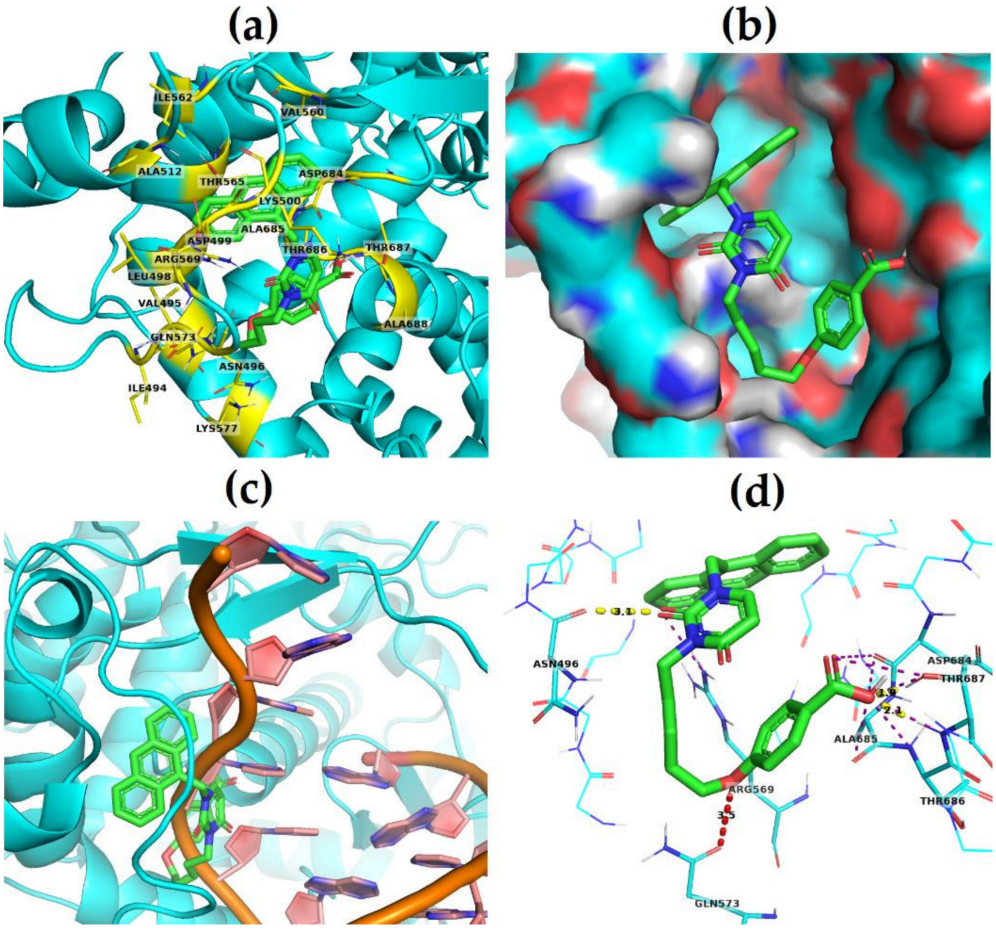

Figure 5. 876 Docked to NSP12. Receptor shown as cyan, ligand as green. (**a**) neighbouring amino acids (yellow), (**b**) pocket surface, (**c**) superposition of original 7EIZ with RNA duplex (brown), (**d**) polar contacts formed by **876** with NSP12 (yellow for H-bonds, red for electrostatic clashes, purple for others).

The best binding poses of the leading compound **876** demonstrate the same structural feature, in that the naphthalene moiety was placed in mostly the hydrophobic pocket in the RNA cleft formed by VAL495, LEU498, LYS500, ALA512, VAL560, THR565, ARG569, and ILE572 (Figure 5a). The pocket corresponds well to the anthracene moiety size (Figure 5b). The remaining part of the **876** molecule demonstrates more diversity in poses but strongly tends to occupy the area of the cleft related to the template RNA strand of the enzyme apo form (Figure 5c). Polar contacts are also observable, e.g., the best scoring pose of **876** shown on Figure 5d reveals polar interactions with several residues, where the strongest ones appear between ligand carboxyl and THR687 (both side chain hydroxyl and backbone amino groups).

According to data showing that **876** can binding with SARS-CoV-2 RdRp, we measured its ability to inhibit the transcriptional activity of a purified SARS-CoV-2 RdRp composed of the NSP12 catalytic subunit and two additional proteins, NSP7 and NSP8. SARS-CoV-2 RdRp activity was inhibited by **876** at 100 μM and 50 μM, by 100% and 60%, respectively (Figure 6).

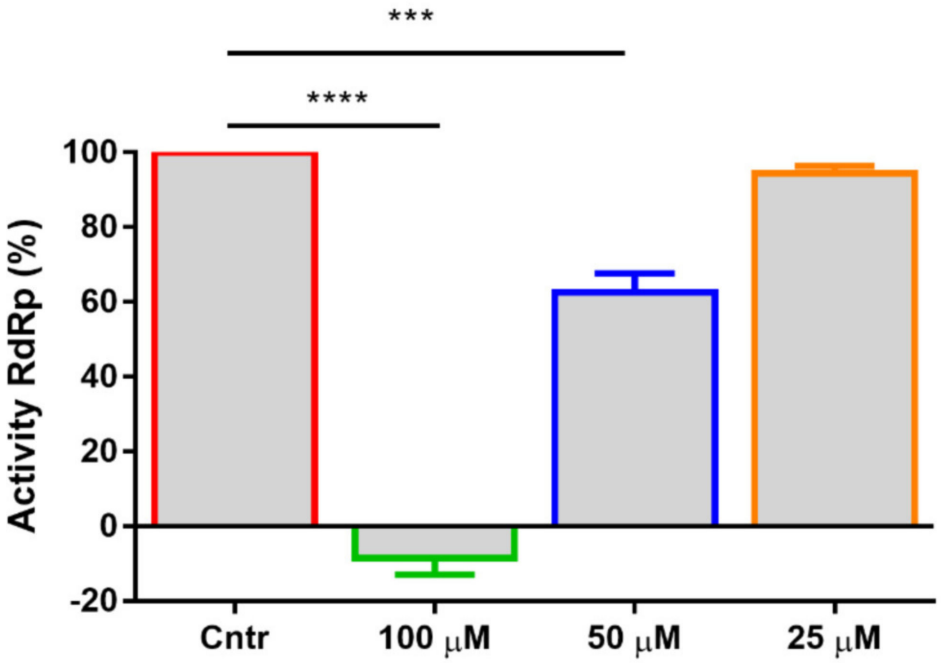

Figure 6. Uracil Derivative **876** Inhibit the Transcriptional Activity of SARS-CoV-2 RNA-dependent RNA polymerase. Transcriptional inhibition plot of the SARS-CoV-2 replication complex treated with **876** or PBS (control) (n = 3). Results are representative mean ± SEM. One-way ANOVA with Tukey's post hoc test: *** $p < 0.001$ and **** $p < 0.0001$.

3. Discussion

The search for inhibitors of SARS-CoV-2 is an important challenge to combat the ongoing COVID-19 pandemic. The widespread use of vaccines to prevent COVID-19 has significantly reduced mortality from COVID-19 among the vaccinated, but the virus continues to circulate and some patients still require hospitalization. The ideal inhibitor of SARS-CoV-2 should be safe for widespread use and effective both early in the course of the disease and later on, reducing the severity of the disease and speeding up recovery. A desirable property would be the ability to reduce the transmission of the virus in a population. In addition, it must have a high threshold of resistance and activity against all circulating strains.

The drugs recommended for treatment with a specific antiviral mechanism of action, including remdesivir, molnupiravir, and nirmatrelvir, were not developed specifically as inhibitors of SARS-CoV-2 and were proposed during the pandemic using the repurpos-

ing mechanism with minimal modifications. They do not sufficiently satisfy the above criteria and have a number of significant drawbacks. Remdesivir, which has a terminating mechanism of action, is an injectable drug used in the clinic to reduce the severity of the disease [28]. The mechanism of action of molnupiravir lies in the mutagenesis of the viral genome, which causes the risks of accelerating the evolution of the virus with its widespread use, as well as its toxicity [29]. Nirmatrelvir, being the most extensively redesigned to inhibit SARS-CoV-2, showed the highest activity [30]. However, the peptide nature of the drug does not allow us to rely on its wide availability for the treatment of patients with COVID-19 in the near future.

The group of non-nucleoside inhibitors studied by us, which are N_1,N_3-disubstituted derivatives of uracil, is distinguished by the simplicity of chemical synthesis. The study of the mechanism of action, taking into account the data of molecular docking and the assessment of polymerase activity in vitro, indicates the ability to inhibit the RNA groove of the RdRp (Nsp12). Taking into account the high conservatism of Nsp12, the manifestation of the inhibitory activity of the compounds against various genetic variants of the virus is not surprising.

The disadvantage of the studied group of N_1,N_3-disubstituted uracil derivatives is the low solubility. Our current efficacy studies using an animal model indicate the need to create a stabilized finished dosage form, leading to an increase in the solubility and bioavailability of the target compounds. Thus, the main tasks in working with this group of compounds are to obtain analogs with increased solubility and the stabilization of molecules in the process of obtaining finished dosage forms for oral administration.

4. Materials and Methods

4.1. General

All reagents were obtained from Sigma and Acros Organics. Anhydrous 1,2-dichloroethane and EtOAc were obtained by distillation over P_2O_5. TLC was performed on Merck TLC Silica gel 60 F_{254} plates eluted with the specified solvents and samples were made visual with a UV lamp, VL-6. LC (Vilber Lourmat, Eberald Zell, Germany). Acros Organics (Acros Organics BV, Geel, Belgium) silica gel (Kieselgur 60–200 μm, 60 A) was used for column chromatography. Yields refer to spectroscopically (^{1}H and ^{13}C NMR) homogeneous material s. Melting points were determined in glass capillaries on a Mel-Temp 3.0 (Laboratory Devices Inc., Auburm, CA, USA).

4.2. General Procedure for the Synthesis of Acids **601**, **870**, **871**, **872**, **873** *and* **874**

A mixture 1.416 mmol of 1-substituted uracil (**1**–**10**) and 0.29 g (2.098 mmol) K_2CO_3 in a solution of 10 mL of DMF was stirred at 80 °C for 1 h, and 1.40 mmol of 4-(ω-bromoalkoxy) benzoic acid methyl ester (**11**–**13**) was added and stirred at the same temperature for 24 h. Then, the reaction mass was evaporated in a vacuum, water (100 mL) was added to the residue, it was extracted with 1,2-dichloroethane (4 × 25 mL), and the extract was evaporated under reduced pressure. The residue was purified by flash chromatography followed by evaporation of the eluent under reduced pressure. The residue was dissolved in a mixture of ethanol (50 mL) and water (30 mL), 0.3 g (7.500 mmol) of NaOH was added, and the resulting mixture was stirred at room temperature for two days. Ethanol was evaporated under reduced pressure, the residue was diluted with water (200 mL) and then it was acidified with hydrochloric acid to pH 2. The precipitate was filtered off, dried in air, and crystallized from an ethyl acetate–hexane mixture (2:1).

NMR spectra were obtained using Bruker Avance 400 (400 MHz for ^{1}H and 100 MHz for ^{13}C) spectrometer in DMSO-d6 or CDCl3 with tetramethylsilane as an internal standard.

4-[4-[2,6-Dioxo-3-(naphthyl-1-methyl)-3,6-dihydropyrimidin-1(^{2}*H*)-yl] butoxy]benzoic acid (**601**). Yield 76%, mp 183–184.5 °C, R_f 0.52 (i-PrOH-ethyl acetate-NH4OH, 9:6:5); ^{1}H NMR (400 Hz, $CDCl_3$), δ, ppm: 1.67 (^{2}H, quin, J = 8.2 Hz, CH_2), 1.88 (^{2}H, quin, J = 7.9 Hz, CH_2), 4.01–4.08 (^{4}H, m, CH_2 × 2), 5.32 (^{2}H, s, CH_2), 5.64 (^{1}H, d, J = 8.1 Hz, uracil H-5), 6.91 (^{1}H, d, J = 8.9 Hz, H-3′, H-5′), 6.99 (^{1}H, d, J = 7.9 Hz, uracil H-6), 7.36–7.48 (^{2}H, m, aromatic

H), 7.50–7.57 (^{2}H, m, aromatic H), 7.87–7.95 (^{3}H, m, aromatic H), 8.03 (^{2}H, d, J = 8.9 Hz, H-2′, H-6′). ^{13}C NMR (100 MHz, $CDCl_3$), δ, ppm: 23.5, 27.4, 41.4, 49.3, 68.0, 102.4, 112.7, 116.4, 123.4, 124.7, 127.7, 128.0, 128.2, 128.5, 129.5, 130.7, 132.3, 132.5, 140.5, 151.8, 158.3, 162.7.

4-[5-[3-[5-(4-Fluorophenoxy)pentyl]-2,6-dioxo-3,6-dihydropyrimidin-1(^{2}*H*)-yl]pentyloxy] benzoic acid (**870**). Yield 88%, mp 133–135 °C, R_f 0.54 (i-PrOH-ethyl acetate-NH_4OH, 9:6:5); ^{1}H NMR (400 Hz, DMSO-d_6), δ, ppm: 1.36–1.39 (^{4}H, m, $CH_2 \times 2$), 1.55–1.75 (^{8}H, m, $CH_2 \times 4$), 3.69–4.00 (^{8}H, m, $CH_2 \times 4$), 5.66 (^{1}H, d, J = 7.8 Hz, uracil H-5), 6.87 (^{2}H, d, J = 9 Hz, H-3′, H-5′), 6.90 (^{2}H, d, J = 8.9 Hz, H-3″, H-5″), 6.97 (^{2}H, d, J = 7.9 Hz, H-2″, H-6″), 7.68 (^{1}H, d, J = 7.8 Hz, uracil H-6), 7.86 (^{2}H, d, J = 8.9 Hz, H-2′, H-6′). ^{13}C NMR (100 MHz, DMSO-d_6), δ, ppm: 22.4, 22.8, 26.8, 28.1, 28.2, 28.3, 48.5, 67.6, 67.7, 100.1, 114.2, 115.5, 115.6, 115.7, 115.9, 122.8, 131.4, 144.1, 151.0, 155.0, 155.2, 157.6, 162.3, 162.4, 167.1.

4-[5-[3-[5-(2-Bromophenoxy)pentyl]-2,6-dioxo-3,6-dihydropyrimidin-1(^{2}*H*)-yl]pentyloxy] benzoic acid (**871**). Yield 84%, mp 91–92 °C, R_f 0.55 (i-PrOH-ethyl acetate-NH_4OH, 9:6:5); ^{1}H NMR (400 Hz, DMSO-d_6), δ, ppm: 1.36–1.45 (^{4}H, m, $CH_2 \times 2$), 1.61–1.77 (^{8}H, m, $CH_2 \times 4$), 3.70–4.01 (^{8}H, m, $CH_2 \times 4$), 5.65 (^{1}H, d, J = 7.8 Hz, uracil H-5), 6.84 (^{1}H, dt, J = 6.8 and 1.2 Hz, H-4′), 6.96 (^{1}H, d, J = 8.8 Hz, H-3″, H-5″), 7.04 (^{1}H, dd, J = 8.2 and 1.3 Hz, H-6′), 7.28 (^{1}H, dt, J = 1.6 and 7.0 Hz, H-5′), 7.52 (^{1}H, dd, J = 7.9 and 1.6 Hz, H-3′), 7.67 (^{1}H, d, J = 7.8 Hz, uracil H-6), 7.86 (^{2}H, d, J = 8.8 Hz, H-2″, H-6″). ^{13}C NMR (100 MHz, DMSO-d_6), δ, ppm: 22.4, 22.8, 26.8, 28.0, 28.1, 28.2, 48.5, 67.6, 68.2, 100.1, 111.1, 113.7, 114.2, 121.9, 122.8, 129.0, 131.4, 132.9, 144.1, 151.0, 154.8, 162.3, 162.4, 167.1.

4-[5-[3-[5-(2-Bromophenoxy)pentyl]-2,6-dioxo-5-methyl-3,6-dihydropyrimidin-1(^{2}*H*)-yl]pentyloxy]benzoic acid (**872**). Yield 81%, mp 132–134 °C, R_f 0.53 (i-PrOH-ethyl acetate-NH_4OH, 9:6:5); ^{1}H NMR (400 Hz, DMSO-d_6), δ, ppm: 1.38–1.46 (^{4}H, m, $CH_2 \times 2$), 1.60–1.75 (^{8}H, m, $CH_2 \times 4$), 3.62–4.08 (^{8}H, m, $CH_2 \times 4$), 6.89 (^{2}H, d, J = 9 Hz, H-3′, H-5′), 6.91 (^{2}H, d, J = 8.9 Hz, H-3″, H-5″), 6.99 (^{2}H, d, J = 7.9 Hz, H-2″, H-6″), 7.42 (^{2}H, d, J = 9.1 Hz, H-2′, H-6′), 7.53 (^{1}H, s, H-6). ^{13}C NMR (100 MHz, DMSO-d_6), δ, ppm: 12.8, 22.7, 22.9, 26.9, 28.1, 28.2, 28.4, 48.5, 67.6, 67.7, 100.1, 114.2, 115.5, 115.6, 115.7, 115.9, 122.8, 131.4, 144.1, 151.0, 155.0, 155.2, 157.6, 162.3, 162.4, 167.1.

4-[4-[3-[3-(4-Bromophenoxy)propyl]-2,6-dioxo-3,6-dihydropyrimidin-1(^{2}*H*)-yl]butoxy] benzoic acid (**873**). Yield 79%, mp 122–124 °C, R_f 0.51 (i-PrOH-ethyl acetate-NH_4OH, 9:6:5); ^{1}H NMR (400 Hz, DMSO-d_6), δ, ppm: 1.58 (^{2}H, quin, J = 7.3 Hz, CH_2), 1.66 (2H, quin, J = 7.5 Hz, CH_2), 2.01 (^{2}H, quin, J = 6.2 Hz, CH_2), 3.69 (^{2}H, t, J = 7.1 Hz, NCH_2), 3.89 (^{2}H, t, J = 6.4 Hz, OCH_2), 3.99 (^{2}H, t, J = 6.7 Hz, N(3)CH_2), 4.09 (^{2}H, t, J = 5.9 Hz, OCH_2), 5.53 (^{1}H, d, J = 7.8 Hz, uracil H-5), 6.72 (^{1}H, d, J = 8.8 Hz, H-3″, H-5″), 6.87 (^{2}H, d, J = 9.0 Hz, H-3′, H-5′), 7.04 (^{2}H, d, J = 8.8 Hz, H-2″, H-6″), 7.43 (^{2}H, d, J = 8.9 Hz, H-2′, H-6′), 7.62 (^{1}H, d, J = 7.8 Hz, uracil H-6). ^{13}C NMR (100 MHz, DMSO-d_6), δ, ppm: 22.9, 26.9, 28.4, 31.1, 44.9, 49.9, 68.6, 103.3, 115.4, 120.1, 122.8, 123.5, 125.5, 131.4, 135.5, 148.2, 154.3, 161.0, 165.4, 172.5.

4-[5-[3-[5-(3,5-Dimethylphenoxy)pentyl]-2,6-dioxo-3,6-dihydropyrimidin-1(^{2}*H*)-yl]pentyloxy] benzoic acid (**874**). Yield 81%, mp 103.5–105 °C, R_f 0.57 (i-PrOH-ethyl acetate-NH_4OH, 9:6:5); ^{1}H NMR (400 Hz, DMSO-d_6), δ, ppm: 1.34–1.38 (^{4}H, m, $CH_2 \times 2$), 1.52–1.73 (^{8}H, m, $CH_2 \times 4$), 2.17 (^{6}H, s, $CH_3 \times 2$), 3.68–3.98 (^{8}H, m, $CH_2 \times 4$), 5.64 (^{1}H, d, J = 7.9 Hz, uracil H-5), 6.47 (^{2}H, s, H-2′, H-6′), 6.49 (^{1}H, s, H-4′), 6.95 (^{1}H, d, J = 8.9 Hz, H-3″, H-5″), 7.64 (^{1}H, d, J = 7.8 Hz, uracil H-6), 7.85 (^{2}H, d, J = 8.8 Hz, H-2″, H-6″). ^{13}C NMR (100 MHz, DMSO-d_6), δ, ppm: 21.1, 22.5, 26.8, 28.1, 28.2, 28.4, 47.5, 67.6, 67.7, 100.8, 114.2, 115.5, 115.6, 115.7, 115.9, 122.8, 131.4, 144.1, 151.0, 155.0, 155.2, 157.6, 162.3, 162.4, 167.1.

4-[[5-[3-(Anthracen-9-ylmethyl)-2,6-dioxo-3,6-dihydropyrimidin-1(^{2}*H*)-yl]pentyloxy] benzoic acid (**876**). Yield 76%, mp 173–176 °C, R_f 0.52 (i-PrOH-ethyl acetate-NH_4OH, 9:6:5); ^{1}H NMR (400 Hz, $CDCl_3$), δ, ppm: 1.31 (^{2}H, quin, J = 6.8 Hz, CH_2), 1.59 (^{2}H, quin, J = 7.6 Hz, CH_2), 1.67 (^{2}H, quin, J = 7.6 Hz, CH_2), 3.54 (^{2}H, t, J = 7.1 Hz, NCH_2), 3.77 (^{2}H, t, J = 6.1 Hz, OCH_2), 5.68 (^{1}H, d, J = 7.8 Hz, uracil H-5), 6.13 (^{2}H, s, CH_2), 6.72 (^{1}H, d, J = 8.8 Hz, H-3′, H-5′), 6.92 (^{1}H, t, J = 7.6 Hz, uracil H-6), 7.00 (^{2}H, d, J = 8.8 Hz, H-2′, H-6′), 7.45 (^{2}H, t, J = 6.8 Hz, H-3″, H-6″), 7.54 (^{2}H, t, J = 6.8 Hz, H-2″, H-7″), 7.98 (^{2}H, d, J = 8.3 Hz, H-1″, H-8″), 8.41 (^{1}H, s, H-10″), 8.53 (^{2}H, d, J = 9.1 Hz, H-4″, H-5″). ^{13}C NMR (100 MHz, DMSO-d_6),

δ, ppm: 22.4, 23.8, 26.1, 42.5, 45.1, 67.5, 101.0, 114.3, 122.9, 123.5, 125.5, 127.6, 129.4, 130.9, 131.1, 131.4, 141.0, 151.5, 162.0, 162.3, 167.1.

4-[4-[2,6-Dioxo-3-(naphthyl-2-methyl)-3,6-dihydropyrimidin-1(^2H)-yl]butoxy]benzoic acid (**1005**). Yield 72%, mp 143.5–145 °C, R_f 0.52 (i-PrOH-ethyl acetate-NH_4OH, 9:6:5); ^{1}H NMR (400 Hz, DMSO-d_6), δ, ppm: 1.66–1.70 (^{4}H, m, CH_2 × 2), 3.86 (^{2}H, t, J = 7.3 Hz, NCH_2), 4.00 (^{2}H, t, J = 6.4 Hz, OCH_2), 5.09 (^{2}H, s, $ArCH_2$), 5.76 (^{1}H, d, J = 7.9 Hz, uracil H-5), 6.95 (^{2}H, d, J = 9.0 Hz, H-3′, H-5′), 7.43–7.50 (^{3}H, m, aromatic H), 7.79 (^{1}H, s, H-1″), 7.85–7.89 (^{6}H, m, J = 7.9 Hz, uracil H-6, aromatic H). ^{13}C NMR (100 MHz, DMSO-d_6), δ, ppm: 23.9, 26.1, 51.7, 67.4, 100.8, 114.2, 122.9, 125.5, 126.2, 126.5, 127.6, 127.8, 128.4, 131.4, 132.4, 132.8, 134.3, 144.2, 151.3, 162.2, 162.5, 167.1.

4-[4-[3-(4-Bromonaphthyl-1-methyl)-2,6-dioxo-3,6-dihydropyrimidin-1(2*H*)-yl] butoxy] benzoic acid (**1006**). Yield 69%, mp 195.5–197.5 °C, R_f 0.52 (i-PrOH-ethyl acetate-NH_4OH, 9:6:5); 1H NMR (400 Hz, $CDCl_3$), δ, ppm: 1.73 (^{2}H, quin, J = 8.0 Hz, CH_2), 1.88 (^{2}H, quin, J = 7.9 Hz, CH_2), 3.92 (^{2}H, t, J = 6.4 Hz, NCH_2), 4.03 (^{2}H, t, J = 7.5 Hz, OCH_2), 5.34 (^{2}H, s, $ArCH_2$), 5.63 (^{1}H, d, J = 8.0 Hz, uracil H-5), 6.75 (^{1}H, d, J = 9.1 Hz, H-3′, H-5′), 6.97 (^{1}H, d, J = 7.9 Hz, aromatic H), 7.19 (^{1}H, d, J = 7.6 Hz, aromatic H), 7.34 (^{2}H, d, J = 9.0 Hz, H-2′, H-6′), 7.57–7.65 (^{2}H, m, aromatic H), 7.76 (^{1}H, d, J = 7.7 Hz, uracil H-6), 7.94 (^{1}H, dd, J = 7.7 and 1.4 Hz, aromatic H), 8.32 (^{1}H, dd, J = 7.8 and 1.4 Hz, aromatic H). ^{13}C NMR (100 MHz, DMSO-d_6), δ, ppm: 23.5, 27.4, 28.9, 49.3, 68.0, 102.4, 112.7, 116.4, 123.4, 124.7, 127.7, 128.0, 128.2, 128.5, 129.5, 130.7, 132.3, 132.5, 140.5, 151.8, 158.3, 162.7.

4-[3-[3-[12-(4-Bromophenoxy)dodecyl]-2,6-dioxo-3,6-dihydropyrimidin-1(^2H)-yl]propoxy] benzoic acid (**1007**). Yield 54%, mp 110–112 °C, R_f 0.56 (i-PrOH-ethyl acetate-NH_4OH, 9:6:5); ^{1}H NMR (400 Hz, $CDCl_3$), δ, ppm: 1.23–1.31 (^{16}H, m, CH_2 × 8), 1.34–1.39 (^{6}H, m, CH_2 × 3), 3.74–3.77 (^{4}H, m, CH_2 × 2), 3.91–3.94 (^{4}H, m, CH_2 × 2), 5.71 (^{1}H, d, J = 7.9 Hz, uracil H-5), 6.88 (^{1}H, d, J = 9.1 Hz, H-3′, H-5′), 7.41 (^{2}H, d, J = 9.1 Hz, H-2′, H-6′), 7.64 (^{1}H, d, J = 7.8 Hz, uracil H-6). ^{13}C NMR (100 MHz, $CDCl_3$), δ, ppm: 22.6, 25.4, 26.2, 26.8, 27.0, 28.5, 28.6, 28.7, 28.9, 49.6, 67.7, 100.1, 111.6, 116.7, 128.0, 128.2, 128.4, 129.5, 132.0, 132.3, 132.5, 140.5, 144.4, 151.0, 157.9, 162.3, 169.3.

4-[[5-[3-[5-(4-Bromophenoxy)pentyl]-2,6-dioxo-3,6-dihydropyrimidin-1(^2H)-yl]methyl] benzoic acid (**875**). A mixture of 0.5 g (1.416 mmol) of 1-[5-(4-bromophenoxy)pentyl]uracil (**8**) and 0.3 g (2.171 mmol) of K_2CO_3 in DMF solution (10 mL) was stirred at 80 °C for 1 h, cooled to room temperature, and 0.32 g (1.397 mmol) of 4-chloromethylbenzoic acid methyl ester (**15**) was added and stirred at room temperature for 24 h. Then, the reaction mass was evaporated in a vacuum, the residue was treated with 100 mL of water, extracted with 1,2-dichloroethane (4 × 25 mL) and the extract was evaporated under reduced pressure. The residue was purified by performing flash chromatography, followed by evaporation of the eluent under reduced pressure. The residue was dissolved in a mixture of ethanol (50 mL) and water (30 mL), 0.3 g (7.5 mmol) of NaOH was added, and the resulting mixture was stirred at room temperature for two days. Ethanol was evaporated under reduced pressure, the residue was diluted with water (200 mL) and acidified with hydrochloric acid to pH 2. The precipitate that formed was filtered, dried in air, and the product was crystallized from an ethyl acetate–hexane mixture. (3:1). Yield 77%, mp 186–187 °C, R_f 0.52 (i-PrOH-ethyl acetate-NH_4OH, 9:6:5); ^{1}H NMR (400 Hz, DMSO-d_6), δ, ppm: 1.36 (^{2}H, quin, J = 8.1 Hz, CH_2), 1.61 (^{2}H, quin, J = 7.3 Hz, CH_2), 1.70 (^{2}H, quin, J = 7.6 Hz, CH_2), 3.65 (^{2}H, t, J = 7.2 Hz, NCH_2), 3.92 (^{2}H, t, J = 6.5 Hz, OCH_2), 5.04 (^{2}H, s, $ArCH_2$), 5.53 (^{1}H, d, J = 7.8 Hz, uracil H-5), 6.76 (^{1}H, d, J = 9.1 Hz, H-3′, H-5′), 7.34 (^{1}H, d, J = 8.3 Hz, H-3″, H-5″), 7.41 (^{2}H, d, J = 8.8 Hz, H-2′, H-6′), 7.64 (^{1}H, d, J = 7.8 Hz, uracil H-6), 7.88 (^{2}H, d, J = 8.3 Hz, H-2″, H-6″). ^{13}C NMR (100 MHz, DMSO-d_6), δ, ppm: 22.4, 28.2, 47.3, 50.2, 67.5, 100.8, 111.8, 116.7, 132.1, 132.5, 134.4, 145.7, 151.0, 157.9, 163.8, 169.6.

1-(Anthracen-9-ylmethyl)-3-[6-(4-bromophenoxy)hexyl]uracil (**611**). A mixture of 0.5 g (1.643 mmol) 1-(anthracen-9-ylmethyl)uracil (**4**) and 0.29 g (2.098 mmol) K_2CO_3 in a DMF (10 mL) solution was stirred at 80 °C for 1 h, 0.56 g (1.666 mmol) of 1-bromo-(6-bromohexyloxy)benzene methyl ester (**16**) and stirred at the same temperature for 24 h. Then, the reaction mass was evaporated in a vacuum, the residue was extracted with

1,2-dichloroethane (4 × 25 mL) and the extract was evaporated under reduced pressure. The residue was purified by performing flash chromatography, followed by evaporation of the eluent under reduced pressure. The residue was crystallized from ethyl acetate–hexane (3:1). Yield 66%, mp 109.5–111 °C, R_f 0.68 (1,2-dichloroethane-ethyl acetate, 1:1); ^{1}H NMR (400 Hz, $CDCl_3$), δ, ppm: 1.31 (^{2}H, quin, J = 6.8 Hz, CH_2), 1.59 (^{2}H, quin, J = 7.6 Hz, CH_2), 1.67 (^{2}H, quin, J = 7.6 Hz, CH_2), 3.54 (^{2}H, t, J = 7.1 Hz, NCH_2), 3.77 (^{2}H, t, J = 6.1 Hz, OCH_2), 5.68 (^{1}H, d, J = 7.8 Hz, uracil H-5), 6.13 (^{2}H, s, CH_2), 6.72 (^{1}H, d, J = 8.8 Hz, H-3′, H-5′), 6.93 (^{1}H, t, J = 7.6 Hz, uracil H-6), 7.37 (^{2}H, d, J = 8.8 Hz, H-2′, H-6′), 7.45 (^{2}H, t, J = 6.8 Hz, H-3″, H-6″), 7.54 (^{2}H, t, J = 6.8 Hz, H-2″, H-7″), 7.98 (^{2}H, d, J = 8.3 Hz, H-1″, H-8″), 8.41 (^{1}H, s, H-10″), 8.53 (^{2}H, d, J = 9.1 Hz, H-4″, H-5″). ^{13}C NMR (100 MHz, $CDCl_3$), δ, ppm: 22.7, 27.4, 28.47, 28.51, 38.4, 49.2, 67.4, 101.3, 112.6, 116.1, 124.6, 124.7, 125.8, 127.9, 128.2, 129.0, 131.0, 131.2, 132.1, 142.1, 151.3, 157.9, 163.5.

4.3. Cells and Viruses

African green monkey kidney Vero E6 cells (ATCC®-1586) were propagated in DMEM (Gibco, Gaithersburg, MD, USA) supplemented with 1% (*v*/*v*) penicillin/streptomycin solution (Gibco, USA) and heat-inactivated 10% (*v*/*v*) fetal bovine serum (FBS) (HyClone, Logan, UT, USA). In this study, we used the following SARS-CoV-2 strains: the Delta variant B.1.617.2 (hCoV-19/Russia/MOW-Moscow_PMVL-49/2021; EPI_ISL_4572812), the Beta variant B.1.351 (hCoV-19/Netherlands/NoordHolland_10159/2021; Ref-SKU: 014V-04058), and the Omicron variant BA.1 (hCoV-19/Russia/MOW-Moscow_PMVL-O16/2021; EPI_ISL_7263933). The viruses were isolated from oro/nasopharyngeal swabs and propagated in Vero E6. All experiments using infectious SARS-CoV-2 were performed in a biosafety level 3 (BSL3) laboratory.

4.4. Cytopathic Effect Inhibition Antiviral Assay

Vero E6 cells (2×10^4 cells/well) were seeded into 96-wells plates and treated with different concentrations of test compounds (1:4 serial dilutions, from 100 to 0.097 μM). Each compound concentration was evaluated for both antiviral efficacy and cytotoxicity. Then, the cells were infected with SARS-CoV-2 at 100$TCID_{50}$. Cell cultures were incubated at 37 °C in 5% CO_2 for 72 h prior to assessment of the virus-induced cytopathic effect (CPE). CPE and cytotoxicity of the compound were determined using an MTT assay as described recently [31].

4.5. Plaque Reduction Assay

A plaque reduction assay was performed to plot the 50% inhibitory concentration (IC_{50}) of individual compounds against the Omicron variant of SARS-CoV-2 as described in [32] with some modifications. Vero E6 cells were seeded at 3×10^4 cells per well in 96-well plates the day before the assay. After 18 h of incubation, 50 p.f.u. SARS-CoV-2 in the presence or absence of compounds was added to the cell monolayer, and the plates were incubated for an additional 1 h at 37 °C in 5% CO_2 before removing unbound viral particles by removing the medium and washing with PBS. Monolayers were then overlaid with DMEM containing 0.7% carboxymethylcellulose (CMC, Sigma, St. Louis, MO, USA) with appropriate concentrations of the individual compounds, and then incubated for an additional 72 h. Then, the wells were fixed with 10% formaldehyde and CMC was removed. Monolayers were stained with 0.5% crystal violet (Sigma, St. Louis, MO, USA) and plaques were counted. The percent of inhibition of plaque formation relative to control wells (without compounds) was determined for each test compound concentration.

4.6. Time-of-Addition Experiments

The assays were performed as described previously [31]. Briefly, Vero E6 cells were seeded into 96-well plates and treated with **874** or **876** (25 μM) at different stages of virus infection (full-time, entry and post-entry). The cells were infected with SARS-CoV-2 (MOI = 0.01) and then incubated for 1 h. The viral inoculum was then removed, and the

cells were washed twice with PBS. At 18 h post-infection, the cell culture supernatant of each time point experiment was collected for viral yield measurements using qRT–PCR, as described in [31,33].

4.7. Molecular Docking

Molecular docking studies were performed on the set of compounds for the SARS-CoV-2 RdRp main protein (NSP12) using Smina software [34] and an AutoDock Vina fork [35]. Several structures of SARS-CoV-2 RdRp are currently available on RCSB.org, including different combinations of cofactors (replicative complex member proteins, RNA and ligands). In our study, we used the NSP12 structure from PDB ID 7EIZ (CryoEM structure of the replicative complex including RNA duplex fragment) [36]. We removed the RNA duplex from the cleft before docking. A ~9700 A3 grid box was used, including the cleft itself. Chain A (NSP12) from 7EIZ was prepared using the pdb2pqr 3.0 tool [37,38] with default parameters (pH 7.0, AMBER force field). Then, it was converted to a pdbqt format using the prepare_receptor script from ADFRsuite version 1.0 [39]. Ligands were converted to the pdbqt format using the prepare_ligand script included in the same suite. The docking procedure was repeated 4 times with a random initial seed to gather statistics. Poses with best score values (kcal/mol) were taken from each run. Structures were visualized using PyMol [40].

4.8. Inhibition Activity of SARS-CoV-2 RNA-Dependent RNA Polymerase (RdRp)

The activity of SARS-CoV-2 RdRp was assessed using the SARS-CoV-2 RNA-dependent RNA polymerase kit plus (Profoldin #S2RPA100KE), according to the manufacture instructions. In brief, reactions were carried out at 35 °C for 2 h in the presence or absence (control) of the test compound. Then, fluorescent dye was added, and fluorescence was determined using a Qubit fluorimeter (Thermo Fisher, MA, USA). The inhibition of RdRp activity was calculated from the values obtained for control samples.

5. Conclusions

Our study demonstrated in vitro efficacy novel uracil derivatives against SARS-CoV-2 VOCs, including «Omicron». We also found that compound **876** was able to directly inhibit the activity of RdRp. The presented docking results reflect one possible mechanism of RdRp inhibition by the **876** compound. Other compounds also demonstrated the possibility to dock into this pocket but with worse score values. Anthracyl analogs demonstrated lower RMSD between poses and a more advanced fit, suggesting that such a class of compounds may be promising for the design of further SARS-CoV-2 inhibitors. We expect that our findings will serve as a starting point for further testing of the selected candidates in more complex and biologically meaningful preclinical models of SARS-CoV-2 infection as potential antivirals.

6. Patents

Uracil Derivatives with Antiviral Activity Against SARS-CoV-2 RU 2 769 828 (28.12.2021).

Author Contributions: Conceptualization: A.E.S., M.S.N. and V.A.G.; methodology: A.E.S., N.A.K., D.V.V., I.A.I., L.I.R., E.V.S., M.P.P. and E.S.G.; software: A.A.T.; investigation: A.E.S., N.A.K., D.V.V., M.P.P., S.I.L., S.A.Z. and E.S.G.; data curation: V.A.G.; writing—original draft preparation: A.E.S.; writing—review and editing: V.A.G.; supervision: V.A.G., N.A.Z.; resources V.A.G., N.A.Z., D.Y.L., A.L.G.; project administration: N.A.Z., D.Y.L., A.L.G. All authors have read and agreed to the published version of the manuscript.

Funding: This research was funded by Ministry of Health of Russia, grant number 121111200070-4 (P16).

Institutional Review Board Statement: Not applicable.

Informed Consent Statement: Not applicable.

Data Availability Statement: Not applicable.

Acknowledgments: Many thanks to the employees of Gamaleya Center who provided the reagents, as well as for project support from Timofey A. Remizov and Anastasia A. Zakharova.

Conflicts of Interest: The authors declare no conflict of interest.

References

1. Shankar, P.R.; Nadarajah, V.D.; Wilson, I.G. Implications of the ongoing coronavirus disease 2019 pandemic for primary care. *Aust. J. Prim. Health* **2022**, *28*, 200–203. [CrossRef] [PubMed]
2. V'Kovski, P.; Kratzel, A.; Steiner, S.; Stalder, H.; Thiel, V. Coronavirus biology and replication: Implications for SARS-CoV-2. *Nat. Rev. Microbiol.* **2020**, *19*, 155–170. [CrossRef] [PubMed]
3. Stadler, K.; Masignani, V.; Eickmann, M.; Becker, S.; Abrignani, S.; Klenk, H.-D.; Rappuoli, R. SARS—Beginning to understand a new virus. *Nat. Rev. Genet.* **2003**, *1*, 209–218. [CrossRef]
4. Yadav, R.; Chaudhary, J.; Jain, N.; Chaudhary, P.; Khanra, S.; Dhamija, P.; Sharma, A.; Kumar, A.; Handu, S. Role of Structural and Non-Structural Proteins and Therapeutic Targets of SARS-CoV-2 for COVID-19. *Cells* **2021**, *10*, 821. [CrossRef]
5. Markov, P.V.; Katzourakis, A.; Stilianakis, N.I. Antigenic evolution will lead to new SARS-CoV-2 variants with unpredictable severity. *Nat. Rev. Genet.* **2022**, *20*, 251–252. [CrossRef] [PubMed]
6. Mei, M.; Tan, X. Current Strategies of Antiviral Drug Discovery for COVID-19. *Front. Mol. Biosci.* **2021**, *8*, 671263. [CrossRef]
7. Gottlieb, R.L.; Vaca, C.E.; Paredes, R.; Mera, J.; Webb, B.J.; Perez, G.; Oguchi, G.; Ryan, P.; Nielsen, B.U.; Brown, M.; et al. Early Remdesivir to Prevent Progression to Severe COVID-19 in Outpatients. *N. Engl. J. Med.* **2022**, *386*, 305–315. [CrossRef]
8. Jayk Bernal, A.; Gomes da Silva, M.M.; Musungaie, D.B.; Kovalchuk, E.; Gonzalez, A.; Delos Reyes, V.; Martín-Quirós, A.; Caraco, Y.; Williams-Diaz, A.; Brown, M.L.; et al. Molnupiravir for Oral Treatment of COVID-19 in Nonhospitalized Patients. *N. Engl. J. Med.* **2022**, *386*, 509–520. [CrossRef]
9. Hammond, J.; Leister-Tebbe, H.; Gardner, A.; Abreu, P.; Bao, W.; Wisemandle, W.; Baniecki, M.; Hendrick, V.M.; Damle, B.; Simón-Campos, A.; et al. Oral Nirmatrelvir for High-Risk, Nonhospitalized Adults with COVID-19. *N. Engl. J. Med.* **2022**, *386*, 1397–1408. [CrossRef]
10. Usach, I.; Melis, V.; Peris, J.-E. Non-nucleoside reverse transcriptase inhibitors: A review on pharmacokinetics, pharmacodynamics, safety and tolerability. *J. Int. AIDS Soc.* **2013**, *16*, 18567. [CrossRef]
11. Tian, L.; Qiang, T.; Liang, C.; Ren, X.; Jia, M.; Zhang, J.; Li, J.; Wan, M.; YuWen, X.; Li, H.; et al. RNA-dependent RNA polymerase (RdRp) inhibitors: The current landscape and repurposing for the COVID-19 pandemic. *Eur. J. Med. Chem.* **2021**, *213*, 113201. [CrossRef] [PubMed]
12. Saha, S.; Nandi, R.; Vishwakarma, P.; Prakash, A.; Kumar, D. Discovering Potential RNA Dependent RNA Polymerase Inhibitors as Prospective Drugs Against COVID-19: An in Silico Approach. *Front. Pharmacol.* **2021**, *12*, 267. [CrossRef] [PubMed]
13. Wang, M.; Cao, R.; Zhang, L.; Yang, X.; Liu, J.; Xu, M.; Shi, Z.; Hu, Z.; Zhong, W.; Xiao, G. Remdesivir and chloroquine effectively inhibit the recently emerged novel coronavirus (2019-nCoV) in vitro. *Cell Res.* **2020**, *30*, 269–271. [CrossRef] [PubMed]
14. Sheahan, T.P.; Sims, A.C.; Leist, S.R.; Schäfer, A.; Won, J.; Brown, A.J.; Montgomery, S.A.; Hogg, A.; Babusis, D.; Clarke, M.O.; et al. Comparative therapeutic efficacy of remdesivir and combination lopinavir, ritonavir, and interferon beta against MERS-CoV. *Nat. Commun.* **2020**, *11*, 222. [CrossRef]
15. Menéndez-Arias, L. Mechanisms of resistance to nucleoside analogue inhibitors of HIV-1 reverse transcriptase. *Virus Res.* **2008**, *134*, 124–146. [CrossRef] [PubMed]
16. Paton, N.I.; Kityo, C.; Thompson, J.; Nankya, I.; Bagenda, L.; Hoppe, A.; Hakim, J.; Kambugu, A.; van Oosterhout, J.J.; Kiconco, M.; et al. Nucleoside Reverse-Transcriptase Inhibitor Cross-Resistance and Outcomes from Second-Line Antiretroviral Therapy in the Public Health Approach: An Observational Analysis within the Randomised, Open-Label, EARNEST Trial. *Lancet HIV* **2017**, *4*, e341–e348. [CrossRef]
17. Paramonova, M.P.; Snoeck, R.; Andrei, G.; Khandazhinskaya, A.L.; Novikov, M.S. New acetamide derivatives containing (ω-p-bromophenoxyalkyl)uracil moiety and their anticytomegalovirus activity. *Mendeleev Commun.* **2020**, *30*, 602–603. [CrossRef]
18. Babkov, D.A.; Khandazhinskaya, A.L.; Chizhov, A.O.; Andrei, G.; Snoeck, R.; Seley-Radtke, K.L.; Novikov, M.S. Toward the discovery of dual HCMV–VZV inhibitors: Synthesis, structure activity relationship analysis, and cytotoxicity studies of long chained 2-uracil-3-yl-N-(4-phenoxyphenyl)acetamides. *Bioorg. Med. Chem.* **2015**, *23*, 7035–7044. [CrossRef]
19. Novikov, M.S.; Ivanova, O.N.; Ivanov, A.V.; Ozerov, A.A.; Valuev-Elliston, V.T.; Temburnikar, K.; Gurskaya, G.V.; Kochetkov, S.N.; Pannecouque, C.; Balzarini, J.; et al. 1-[2-(2-Benzoyl- and 2-benzylphenoxy)ethyl]uracils as potent anti-HIV-1 agents. *Bioorg. Med. Chem.* **2011**, *19*, 5794–5802. [CrossRef]
20. Magri, A.; Ozerov, A.; Tunitskaya, V.L.; Valuev-Elliston, V.T.; Wahid, A.; Pirisi, M.; Simmonds, P.; Ivanov, A.V.; Novikov, M.S.; Patel, A.H. Exploration of acetanilide derivatives of 1-(ω-phenoxyalkyl)uracils as novel inhibitors of Hepatitis C Virus replication. *Sci. Rep.* **2016**, *6*, 29487. [CrossRef]
21. Sapozhnikova, K.A.; Slesarchuk, N.A.; Orlov, A.A.; Khvatov, E.V.; Radchenko, E.V.; Chistov, A.A.; Ustinov, A.V.; Palyulin, V.A.; Kozlovskaya, L.I.; Osolodkin, D.I.; et al. Ramified derivatives of 5-(perylen-3-ylethynyl)uracil-1-acetic acid and their antiviral properties. *RSC Adv.* **2019**, *9*, 26014–26023. [CrossRef] [PubMed]
22. Baker, B.R.; Kelley, J.L. Irreversible Enzyme Inhibitors. CLXXI. Inhibition of FUDR Phosphorylase from Walker 256 Rat Tumor by 5-Substituted Uracils. *J. Med. Chem.* **1970**, *13*, 461–467. [CrossRef] [PubMed]

23. Malik, V.; Singh, P.; Kumar, S. Regioselective synthesis of 1-allyl- and 1-arylmethyl uracil and thymine derivatives. *Tetrahedron* **2005**, *61*, 4009–4014. [CrossRef]
24. Novikov, M.S.; Babkov, D.A.; Paramonova, M.P.; Khandazhinskaya, A.L.; Ozerov, A.A.; Chizhov, A.O.; Andrei, G.; Snoeck, R.; Balzarini, J.; Seley-Radtke, K.L. Synthesis and anti-HCMV activity of 1-[ω-(phenoxy)alkyl]uracil derivatives and analogues thereof. *Bioorg. Med. Chem.* **2013**, *21*, 4151–4157. [CrossRef] [PubMed]
25. Paramonova, M.P.; Ozerov, A.A.; Chizhov, A.O.; Snoeck, R.; Andrei, G.; Khandazhinskaya, A.L.; Novikov, M.S. Synthesis of uracil–coumarin conjugates as potential inhibitors of virus replication. *Mendeleev Commun.* **2019**, *29*, 638–639. [CrossRef]
26. Paramonova, M.P.; Babkov, D.A.; Valuev-Elliston, V.T.; Ivanov, A.V.; Kochetkov, S.N.; Pannecouque, C.; Ozerov, A.A.; Balzarini, J.; Novikov, M.S. Synthesis and Anti-HIV-1 Activity of 1-[ω-(Phenoxy)Alkyl and -Alkenyl]Uracil Derivatives. *Pharm. Chem. J.* **2013**, *47*, 459–463. [CrossRef]
27. Shi, Y.; Zhang, X.; Mu, K.; Peng, C.; Zhu, Z.; Wang, X.; Yang, Y.; Xu, Z.; Zhu, W. D3Targets-2019-nCoV: A webserver for predicting drug targets and for multi-target and multi-site based virtual screening against COVID-19. *Acta Pharm. Sin. B* **2020**, *10*, 1239–1248. [CrossRef]
28. Grein, J.; Ohmagari, N.; Shin, D.; Diaz, G.; Asperges, E.; Castagna, A.; Feldt, T.; Green, G.; Green, M.L.; Lescure, F.-X.; et al. Compassionate Use of Remdesivir for Patients with Severe COVID-19. *N. Engl. J. Med.* **2020**, *382*, 2327–2336. [CrossRef]
29. Painter, W.P.; Holman, W.; Bush, J.A.; Almazedi, F.; Malik, H.; Eraut, N.C.J.E.; Morin, M.J.; Szewczyk, L.J.; Painter, G.R. Human Safety, Tolerability, and Pharmacokinetics of Molnupiravir, a Novel Broad-Spectrum Oral Antiviral Agent with Activity against SARS-CoV-2. *Antimicrob. Agents Chemother.* **2021**, *65*, e02428-20. [CrossRef]
30. Owen, D.R.; Allerton, C.M.N.; Anderson, A.S.; Aschenbrenner, L.; Avery, M.; Berritt, S.; Boras, B.; Cardin, R.D.; Carlo, A.; Coffman, K.J.; et al. An Oral SARS-CoV-2 Mpro Inhibitor Clinical Candidate for the Treatment of COVID-19. *Science* **2021**, *374*, 1586–1593. [CrossRef]
31. Siniavin, A.E.; Streltsova, M.A.; Nikiforova, M.A.; Kudryavtsev, D.S.; Grinkina, S.D.; Gushchin, V.A.; Mozhaeva, V.A.; Starkov, V.G.; Osipov, A.V.; Lummis, S.C.R.; et al. Snake venom phospholipase A2s exhibit strong virucidal activity against SARS-CoV-2 and inhibit the viral spike glycoprotein interaction with ACE2. *Experientia* **2021**, *78*, 7777–7794. [CrossRef] [PubMed]
32. Yuan, S.; Wang, R.; Chan, J.F.-W.; Zhang, A.J.; Cheng, T.; Chik, K.K.-H.; Ye, Z.-W.; Wang, S.; Lee, A.C.-Y.; Jin, L.; et al. Metallodrug ranitidine bismuth citrate suppresses SARS-CoV-2 replication and relieves virus-associated pneumonia in Syrian hamsters. *Nat. Microbiol.* **2020**, *5*, 1439–1448. [CrossRef] [PubMed]
33. Shidlovskaya, E.V.; Kuznetsova, N.A.; Divisenko, E.V.; Nikiforova, M.A.; Siniavin, A.E.; Ogarkova, D.A.; Shagaev, A.V.; Semashko, M.A.; Tkachuk, A.P.; Burgasova, O.A.; et al. The Value of Rapid Antigen Tests for Identifying Carriers of Viable SARS-CoV-2. *Viruses* **2021**, *13*, 2012. [CrossRef] [PubMed]
34. Koes, D.R.; Baumgartner, M.; Camacho, C.J. Lessons Learned in Empirical Scoring with smina from the CSAR 2011 Benchmarking Exercise. *J. Chem. Inf. Model.* **2013**, *53*, 1893–1904. [CrossRef] [PubMed]
35. Trott, O.; Olson, A.J. AutoDock Vina: Improving the speed and accuracy of docking with a new scoring function, efficient optimization, and multithreading. *J. Comput. Chem.* **2010**, *31*, 455–461. [CrossRef]
36. Yan, L.; Yang, Y.; Li, M.; Zhang, Y.; Zheng, L.; Ge, J.; Huang, Y.C.; Liu, Z.; Wang, T.; Gao, S.; et al. Coupling of N7-methyltransferase and 3′-5′ exoribonuclease with SARS-CoV-2 polymerase reveals mechanisms for capping and proofreading. *Cell* **2021**, *184*, 3474–3485.e11. [CrossRef]
37. Dolinsky, T.J.; Nielsen, J.E.; McCammon, J.A.; Baker, N.A. PDB2PQR: An automated pipeline for the setup of Poisson-Boltzmann electrostatics calculations. *Nucleic Acids Res.* **2004**, *32*, W665–W667. [CrossRef]
38. Dolinsky, T.J.; Czodrowski, P.; Li, H.; Nielsen, J.E.; Jensen, J.H.; Klebe, G.; Baker, N.A. PDB2PQR: Expanding and upgrading automated preparation of biomolecular structures for molecular simulations. *Nucleic Acids Res.* **2007**, *35*, W522–W525. [CrossRef]
39. Morris, G.M.; Huey, R.; Lindstrom, W.; Sanner, M.F.; Belew, R.K.; Goodsell, D.S.; Olson, A.J. AutoDock4 and AutoDockTools4: Automated docking with selective receptor flexibility. *J. Comput. Chem.* **2009**, *30*, 2785–2791. [CrossRef]
40. PyMOL. Available online: https://www.pymol.org/pymol.html? (accessed on 18 June 2022).